

**A98-32439****AIAA-98-2626****NUMERICAL STUDY OF HYPERSONIC TURBULENT FLOW ABOUT SEGMENTED PROJECTILES**

V. V. Riabov\*

*Daniel Webster College**Nashua, New Hampshire 03063-1300, USA*I. V. Yegorov<sup>†</sup> and D. V. Ivanov<sup>‡</sup>*Central Aero-Hydrodynamics Institute**Zhukovsky-3, Moscow region, Russia 140160*

and

H. H. Legner<sup>§</sup>*Physical Sciences Inc.**Andover, Massachusetts 01810, USA*Abstract

The flow structure about a segmented projectile in hypersonic turbulent flow has been studied. The Reynolds-averaged Navier-Stokes equations were solved numerically by application of the implicit monotomized scheme of second-order accuracy, the modified Newton's method, and the Christoffel-Schwarz grid-transformation technique. A strong interference effect has been found. The effect can be characterized by non-monotonous distributions of skin friction, heat flux and pressure along the second segment of the projectile.

Nomenclature $C_f$  = local skin friction coefficient $C_p$  = pressure coefficient $c_p, c_v$  = specific heats at constant pressure and volume $D$  = diameter of the projectile $\mathbf{E}, \mathbf{G}$  = flux-vectors in curvilinear coordinate system, Eqs. (1), (2) $e$  = total energy per unit volume,  $\rho(c_v T + (u^2 + v^2)/2)$  $H$  = total enthalpy per unit volume,  $c_p T + (u^2 + v^2)/2$  $h$  = node size $J$  = Jacobian of the coordinates transformation $k$  = Boltzmann's constant $m$  = molecular mass $Pr$  = Prandtl number $p$  = pressure $\mathbf{Q}$  = vector of dependent variables, Eq. (1) $\mathbf{q}$  = heat flux vector $Re$  = Reynolds number,  $\rho u_\infty D / \mu_\infty$  $r$  = radius of the projectile $s$  = distance along the body surface or along an axis $T$  = temperature $u$  =  $x$ -velocity component $\mathbf{V}$  = velocity vector $v$  =  $y$ -velocity component $x$  = Cartesian  $x$ -coordinate $y$  = Cartesian  $y$ -coordinate $\gamma$  = specific heat ratio,  $c_p/c_v$  $\Delta$  = distance between the segments $\eta$  = curvilinear coordinate $\lambda$  = conductivity coefficient $\lambda_i$  = eigenvalue $\mu$  = viscosity coefficient $\xi$  = curvilinear coordinate $\rho$  = density of fluid $\tau_k$  = regularization parameter, Eq. (17) $\tau_{xy}$  = viscous stress tensor $\phi$  = function, Eq. (11) $\varepsilon$  = small parameter, Eq. (11)Subscripts $c$  = Cartesian coordinate system $w$  = wall value $\infty$  = freestream value

\*Adjunct Associate Professor, Department of Engineering, Mathematics and Sciences. Member AIAA.

†Leading Scientist, Aerothermodynamics Division.

‡Research Scientist, Aerothermodynamics Division.

§Principal Research Scientist, Associate Fellow AIAA.

Copyright © 1998 by the American Institute of Aeronautics and Astronautics, Inc. All rights reserved.

Introduction

The hypersonic projectile studies have been actively revived with recent interest in electromagnetic launchers. Hypervelocity projectile aerophysics, including aerodynamics and flight mechanics, has been reviewed by Reinecke and Legner<sup>1</sup>. Aerothermodynamics of hypersonic non-segmented projectiles has been studied experimentally and numerically by Cayzac et al.<sup>2</sup> Launch perturbation effects in electromagnetic guns were evaluated by Seiler et al.<sup>3</sup> Orphal and Franzén<sup>4</sup> have found that the terminal damage of a hypervelocity projectile can be enhanced if the projectile mass distribution is segmented along its axis.

In the present analysis, hypersonic turbulent flow about two-segment projectile have been studied. The analysis of two-dimensional flow structure is based on numerical solutions of the Reynolds-averaged Navier-Stokes equations using an implicit monotonized scheme of second-order accuracy (Total Variation Diminishing scheme) and Newton's method for solving the grid equations.<sup>5</sup> The technique has been successfully applied by Yegorov, Yegorova, and Riabov<sup>6</sup> and Yegorov et al.<sup>7</sup> in studies of hypersonic viscous flow about bluff cylinders and plates located one after another.

The influence of the Reynolds number and the geometrical factor of interference between the segments,  $\Delta/r$ , on skin-friction, heat flux, velocity, turbulence parameter, pressure and temperature in the flow field and along the surfaces of the projectile has been studied.

Navier-Stokes Equations and Boundary Conditions.

The unsteady two-dimensional Navier-Stokes equations in a curvilinear coordinate system  $(\xi, \eta)$ ,  $x = x(\xi, \eta)$ ,  $y = y(\xi, \eta)$ , where  $x, y$  are Cartesian coordinates have a conservation form:<sup>8,9</sup>

$$\frac{\partial \mathbf{Q}}{\partial t} + \frac{\partial \mathbf{E}}{\partial \xi} + \frac{\partial \mathbf{G}}{\partial \eta} = \mathbf{B} \quad (1)$$

Here  $\mathbf{Q}$  is a dependent-variables vector,  $\mathbf{E}$  and  $\mathbf{G}$  are flux-vectors in curvilinear coordinate system.  $\mathbf{Q}, \mathbf{E}, \mathbf{G}$ , and  $\mathbf{B}$  vectors are corresponding to Cartesian vectors  $\mathbf{Q}_c, \mathbf{E}_c, \mathbf{G}_c$ , and  $\mathbf{B}_c$  as follow:

$$\begin{aligned} \mathbf{Q} &= \mathbf{J} \mathbf{Q}_c; \quad \mathbf{E} = \mathbf{J} \left( \mathbf{E}_c \frac{\partial \xi}{\partial x} + \mathbf{G}_c \frac{\partial \xi}{\partial y} \right) \\ \mathbf{B} &= \mathbf{J} \mathbf{B}_c; \quad \mathbf{G} = \mathbf{J} \left( \mathbf{E}_c \frac{\partial \eta}{\partial x} + \mathbf{G}_c \frac{\partial \eta}{\partial y} \right) \end{aligned} \quad (2)$$

where  $\mathbf{J} = \partial(x,y)/\partial(\xi,\eta)$  is a Jacobian of the coordinates' transformation.

The Cartesian vector components  $\mathbf{Q}_c, \mathbf{E}_c, \mathbf{G}_c$ , and  $\mathbf{B}_c$  for the two-dimensional Navier-Stokes equations have the following form:

$$\begin{aligned} \mathbf{Q}_c &= \begin{pmatrix} \rho \\ \rho u \\ \rho v \\ \rho(e+g^2) \\ \rho g \\ \rho \omega \end{pmatrix}; \quad \mathbf{B}_c = \begin{pmatrix} 0 \\ 0 \\ 0 \\ 0 \\ -h_1 \rho \omega g \\ -h_2 \rho \omega^2 \end{pmatrix} \\ \mathbf{E}_c &= \begin{pmatrix} \rho u \\ \rho u^2 + p + \frac{2}{3} \rho g^2 - \tau_{xx} \\ \rho uv - \tau_{xy} \\ \rho uH - q_x + \frac{5}{3} \rho ug^2 \\ \rho ug - I_x^s \\ \rho u \omega - I_x^\omega \end{pmatrix} \\ \mathbf{G}_c &= \begin{pmatrix} \rho v \\ \rho uv - \tau_{xy} \\ \rho v^2 + p + \frac{2}{3} \rho g^2 - \tau_{yy} \\ \rho vH - q_y + \frac{5}{3} \rho vg^2 \\ \rho vg - I_y^s \\ \rho v \omega - I_y^\omega \end{pmatrix} \end{aligned} \quad (3)$$

The viscous stress tensor  $\tau$  has the components:

$$\begin{aligned} \tau_{xx} &= (\mu + \mu_T) \left( -\frac{2}{3} \text{div} \mathbf{V} + 2 \frac{\partial u}{\partial x} \right) \\ \tau_{xy} = \tau_{yx} &= (\mu + \mu_T) \left( \frac{\partial u}{\partial y} + \frac{\partial v}{\partial x} \right) \\ \tau_{yy} &= (\mu + \mu_T) \left( -\frac{2}{3} \text{div} \mathbf{V} + 2 \frac{\partial v}{\partial y} \right) \end{aligned} \quad (4)$$

The heat flux vector  $\mathbf{q}$  is calculated by formula:

$$\mathbf{q} = (\lambda + \lambda_T) \text{grad}(T) + \tau \mathbf{V} \quad (5)$$

Turbulent viscosity  $\mu_T$  and heat conductivity coefficients  $\lambda_T$  are determined as follow:

$$\begin{aligned} \mathbf{I}^q &= \left( \mu + \frac{\mu_T}{Pr_1} \right) \text{grad}(g) \\ \mathbf{I}^\omega &= \left( \mu + \frac{\mu_T}{Pr_2} \right) \text{grad}(\omega) \\ g &= \sqrt{k}; \quad \omega = \varepsilon/k \end{aligned} \quad (6)$$

The mass-averaged Navier-Stokes equation system (1) for the compressible perfect gas model is completed by the state equation as well as by two equations describing the differential turbulent  $g$ - $\omega$  model offered by Coakley and Huang<sup>10</sup>:

$$\begin{aligned} \mu_T &= C_\mu f \rho g l = C_\mu f \rho \frac{g^2}{\omega}; \quad C_\mu = 0.09 \\ f &= 1 - \exp\left(-\alpha \frac{\rho r_w g}{\mu}\right); \quad \alpha = 0.02 \\ h_1 &= C_{11} \left( C_\mu f \frac{S}{\omega^2} - \frac{2}{3} \frac{\text{div} \mathbf{V}}{\omega} \right) - C_{12} \\ h_2 &= C_{21} \left( C_\mu f \frac{S}{\omega^2} - C_{23} \frac{\text{div} \mathbf{V}}{\omega} \right) - C_{22} \\ S &= \frac{4}{3} \left[ \left( \frac{\partial u}{\partial x} \right)^2 - \frac{\partial u}{\partial x} \frac{\partial v}{\partial y} + \left( \frac{\partial v}{\partial y} \right)^2 \right] \\ &+ \left( \frac{\partial u}{\partial x} + \frac{\partial v}{\partial y} \right)^2 + \frac{4}{3} \beta \left[ \frac{v^2}{v^2} - \frac{v}{y} \left( \frac{\partial u}{\partial x} + \frac{\partial v}{\partial y} \right) \right] \end{aligned} \quad (7)$$

where  $\beta=0$  for two-dimensional problem, and  $\beta=1$  for axisymmetrical one. Other parameters are as follow<sup>11</sup>:

$$\begin{aligned} C_{11} &= C_{12} = 1; \quad C_{22} = 0.833; \quad C_{23} = 2.4 \\ C_{21} &= 0.055 - 0.5f(g, r_w, \rho, \mu) \\ Pr_1 &= Pr_2 = 2 \end{aligned} \quad (8)$$

Also, it is assumed that the coefficient of viscosity is calculated using a power law variation with temperature,  $\mu/\mu_\infty = (T/T_\infty)^{0.7}$ , and the Prandtl number is constant,  $Pr = 0.7$ , and  $Pr_T = 0.9$ .

For further numerical analysis, new non-dimensional parameters in Eqs. (1) - (6) were set up by normalizing the Cartesian coordinates to the characteristic length scale  $r$  (the radius of a cylinder), the Cartesian velocity components - to the upstream velocity  $u_\infty$ , the pressure - to the double value of the dynamic pressure in the upstream flow, and other parameters - to their values in the upstream flow.

To complete the finite-difference system of the Navier-Stokes equations, the following boundary conditions have been used. The no-slip conditions ( $u = v = 0$ ,  $g = 0$ , and  $\partial\omega/\partial n = 0$ ), constant surface temperature ( $T = T_w$ ), and extrapolations of a pressure from inner area nodes (with the condition  $\partial p/\partial \eta = 0$ ) were posed on the body surface. On the outer surface of the computational area around the body, boundary conditions were written in the form of Riemann invariants and determined by the direction of the perturbation expansion<sup>9</sup>.

#### The Approximation of Equations

The construction of a finite-difference scheme to solve the Navier-Stokes equations (1) given in conservation laws form is based upon an integro-interpolation method.<sup>9</sup> The utilization of an integro-interpolation method applied to the solution of the Navier-Stokes equations gives finite-differences conservation laws analogies:

$$\frac{\mathbf{Q}_{j,k}^{n+1} - \mathbf{Q}_{j,k}^n}{\tau} + \frac{\mathbf{E}_{j+1/2,k}^{n+1} - \mathbf{E}_{j-1/2,k}^{n+1}}{h_\xi} + \frac{\mathbf{G}_{j,k+1/2}^{n+1} - \mathbf{G}_{j,k-1/2}^{n+1}}{h_\eta} = \mathbf{B}_{j,k}^{n+1} \quad (9)$$

Here index  $n$  corresponds to time layer number;  $j, k$  - to node numbers along  $\xi$  and  $\eta$ , correspondingly;  $h_\xi, h_\eta$  - to the node sizes. The developed conservative finite-difference scheme is implicit, and this property of the scheme allows one to avoid any restrictions on the iteration time-step caused by the instability of the ordinary difference schemes in the solution of the stiff differential equations.

At semi-integer nodes, the convective components of the flux vectors  $\mathbf{E}$  and  $\mathbf{G}$  were approximated using a

monotonized scheme of Godunov type.<sup>12</sup> The eigenvalues and eigenvectors at semi-integer nodes were calculated by the Roe method<sup>13</sup>, for the approximate solution of the problem of arbitrary discontinuity decay:

$$\mathbf{E}_{j+\frac{1}{2}} = \frac{1}{2}(\mathbf{E}(\mathbf{Q}_L) + \mathbf{E}(\mathbf{Q}_R)) - \mathbf{R}(\mathbf{Q}_{LR}) \Phi(\Lambda_{LR}) \mathbf{R}(\mathbf{Q}_{LR})^{-1} (\mathbf{Q}_R - \mathbf{Q}_L) \quad (10)$$

Here  $\Phi(\Lambda_{LR})$  is a diagonal matrix with elements  $\phi(\lambda_i)$ ; parameters  $\lambda_i$  are the eigenvalues of the operator  $\mathbf{A} = \partial \mathbf{E} / \partial \mathbf{Q}$ ; and  $\mathbf{R}_{LR} = \mathbf{R}(\mathbf{Q}_{LR})$  is a matrix with the columns being the right-hand side eigenvectors of the operator  $\mathbf{A}$ . The function  $\phi(\lambda)$  has the form:

$$\phi(\lambda) = \begin{cases} |\lambda|, & |\lambda| > \varepsilon \\ \frac{\lambda^2 + \varepsilon^2}{2\varepsilon}, & |\lambda| \leq \varepsilon \end{cases} \quad (11)$$

This form satisfies the "entropy" condition (or the criterion) in the choosing of a numerical solution with the correct physical properties.

To increase the order of the finite-difference approximations up to the second order, the Monotone-Upstream-Scheme-for-Conservation-Laws principle of the minimum derivatives<sup>14</sup> was used to interpolate dependent variables on the node side as follows:

$$\begin{aligned} \mathbf{Q}_L &= \mathbf{Q}_j + \frac{1}{2} \min \text{mod}(\mathbf{Q}_j - \mathbf{Q}_{j-1}, \mathbf{Q}_{j+1} - \mathbf{Q}_j), \\ \mathbf{Q}_R &= \mathbf{Q}_j - \frac{1}{2} \min \text{mod}(\mathbf{Q}_{j+1} - \mathbf{Q}_j, \mathbf{Q}_{j+2} - \mathbf{Q}_{j+1}) \end{aligned} \quad (12)$$

The function  $\min \text{mod}(a, b)$  has the form:

$$\min \text{mod}(a, b) = \begin{cases} a, & ab > 0, \quad |a| < |b| \\ b, & ab > 0, \quad |a| \geq |b| \\ 0, & ab \leq 0 \end{cases} \quad (13)$$

The Roe method<sup>13</sup> was utilized to compute eigenvalues and eigenvectors of the  $\mathbf{A}$ -operator in order to solve approximately the Riemann problem of arbitrary discontinuity decay. Parameters  $\Phi(\Lambda_{LR})$ ,  $\mathbf{R}_{LR}$ ,  $\mathbf{R}_{LR}^{-1}$  were calculated by the values of dependent variables, such as:

$$\begin{aligned} u_{LR} &= \frac{u_L \sqrt{\rho_L} + u_R \sqrt{\rho_R}}{\sqrt{\rho_L} + \sqrt{\rho_R}} \\ v_{LR} &= \frac{v_L \sqrt{\rho_L} + v_R \sqrt{\rho_R}}{\sqrt{\rho_L} + \sqrt{\rho_R}} \\ c_{LR} &= \frac{c_L \sqrt{\rho_L} + c_R \sqrt{\rho_R}}{\sqrt{\rho_L} + \sqrt{\rho_R}} \end{aligned} \quad (14)$$

Here the parameter  $c$  indicates the local speed of sound.

The diffusion components of the flux vectors  $\mathbf{E}$  and  $\mathbf{G}$  at the node side were approximated by the second order central difference scheme:

$$\begin{aligned} \frac{\partial \mathbf{U}}{\partial \xi_{j+\frac{1}{2}, k}} &= \frac{\mathbf{U}_{j+1, k} - \mathbf{U}_{j, k}}{h_\xi} \\ \frac{\partial \mathbf{U}}{\partial \eta_{j+\frac{1}{2}, k}} &= \frac{\mathbf{U}_{j+1, k+1} + \mathbf{U}_{j, k+1} - \mathbf{U}_{j+1, k-1} - \mathbf{U}_{j, k-1}}{4h_\eta} \end{aligned} \quad (15)$$

Here the parameter  $\mathbf{U}$  is a vector of non-conservative dependent variables.

The difference scheme pattern used for the approximation of the Reynolds-averaged Navier-Stokes equations consists of 13 nodes. It was found, that the developed implicit nonlinear finite-difference scheme is absolutely stable in the case of the linear problem.

In present study, the numerical algorithm developed for the internal flow modeling<sup>11</sup> has been adopted to study external hypersonic viscous flows. The construction of the computational mesh was made by numerical solution of the Christoffel-Schwarz transformation problem.<sup>15,16</sup> The technique of the mesh adaptation in the boundary layers at high Reynolds numbers<sup>11,17</sup> has been used in this study.

### Solution of Nonlinear Differences Equations

The nonlinear system of grid equations ( $\mathbf{F}(\mathbf{X}) = 0$ , where  $\mathbf{X}$  is a vector of unknown discrete functions) was solved using the modified Newton's method.<sup>5,8,17</sup>

$$\mathbf{X}^{[k+1]} = \mathbf{X}^{[k]} - \tau_{k+1} \mathbf{D}^{-1} \mathbf{F}(\mathbf{X}^{[k]}) \quad (16)$$

Here  $\mathbf{D} = \partial \mathbf{F} / \partial \mathbf{X}$  is the Jacobi matrix;  $k$  is the iteration number. In computations, the regularization parameter  $\tau_k$  was calculated by formula<sup>18</sup>:

$$\tau_{k+1} = \frac{(\Delta \mathbf{X}^{[k]} - \Delta \mathbf{X}^{[k-1]}, \mathbf{X}^{[k]} - \mathbf{X}^{[k-1]})}{(\Delta \mathbf{X}^{[k]} - \Delta \mathbf{X}^{[k-1]})^2} \quad (17)$$

where  $\Delta \mathbf{X}^{[k]}$  is a vector of corrections. The iteration process is convergent with the second order of the convergence rate and  $\tau_k \rightarrow 1$ .

The iteration Jacobi matrix was found by employing the procedure of finite increments of the residual vector of the required grid functions. The approximation of the Navier-Stokes equations determinates the type of the Jacobi  $\mathbf{D}$ -operator, namely, the rarefied structure of triangular matrices and the initial  $7 \times 7$ -dense matrix coincide.

The system of linear algebraic equations obtained in a nonlinearity iteration was solved by expanding the matrix into a product of two triangular matrices  $\mathbf{L}$  and  $\mathbf{U}$ , where  $\mathbf{L}$  is the lower triangular matrix and  $\mathbf{U}$  is the upper triangular matrix, and  $\partial \mathbf{F} / \partial \mathbf{X} = \mathbf{L} * \mathbf{U}$ . This operation was preceded by the analysis of the sparsity structure of matrices  $\mathbf{L}$  and  $\mathbf{U}$ . In order to reduce the total number of the arithmetic operations and economize on RAM, the variables were numbered using the generalized method of nested dissection<sup>19,20</sup>. This technique was successfully used many times in computational experiments and proved its effectiveness and reliability.<sup>9,11</sup>

### Numerical Calculations and Tests

The calculations were mainly performed on the  $201 \times 151$  grid of the H-type. The size of the nodes was automatically reduced near the body surface<sup>11</sup> and in the vicinity of the symmetry axis.

The convergence and accuracy of the numerical solutions were tested by carrying out a series of calculations of hypersonic viscous flow about a cylinder (at Reynolds number  $Re_{\infty} = 10^5$  and Mach number in upstream flow  $M_{\infty} = 5$ ) on the grids of different size. The analysis of the results<sup>5-7,11</sup> showed that the numerical solution of the problem is convergent. Calculations were carried out at the Work Station RS6000/58H.

To improve the convergence rate of the iteration process, the new technique using the Jacobi matrix was used. The method is based upon the usage of a truncated  $3 \times 3$ -dense matrix. The computing time (approximately 3h. 20 min) of each variant was reduced by the factor of three.

### Results

The flowfield around a two-segment projectile was calculated for a Mach number  $M_{\infty} = 6$  and for a Reynolds number  $Re_{\infty} = 10^5, 10^6, \text{ and } 10^7$ . It was assumed that  $\gamma = 1.4$ , and the body surface is isothermal at  $T_w/T_{\infty} = 2$ . The distance between the segments was  $\Delta/D = 1.2$  and  $2.4$ .

The contours of constant values of local Mach number  $M$ , temperature  $T/T_{\infty}$  and velocity at  $Re_{\infty} = 10^6$  and  $\Delta/D = 1.2$  are shown in Figs. 1, 2, and 3, correspondingly. The flow structure changes significantly in the areas between the segments and behind the projectile. The zone between the segments becomes totally subsonic and turbulent. As a result, the hot-gas area near the down-stream segment spreads far up-stream, up to the rear zone of the first segment. Behind the second segment, the wake area becomes narrow and it is filled with hot gas.

The distribution of the turbulence  $g$ -parameter is shown in Fig. 4. The flow near the second segment is turbulent and extremely complex. Density contours in the flow between the segments are shown in Fig. 5. Their pattern is significantly different from the zones with different values of a turbulent  $g$ -parameter.

The distributions of pressure and skin-friction coefficients, and heat flux along the surface of the first segment (the distance  $s$  is calculated from the nose) are shown in Figs. 6, 7, and 8 correspondingly. The developing recirculation zone between the projectile segments influences these aerothermodynamic parameters on the rear surface of the first body considerably. At  $Re_{\infty} = 10^7$ , the flow becomes turbulent. It results in a significant increase

of shear stress and heat flux. The size of the recirculation zone depends on both the distance between the segments and the Reynolds number. The influence of the first factor on the aerodynamic characteristics of the first segment is localized in the rear area.

The pressure distribution between segments is shown in Fig. 9. At  $Re_{ar} \geq 10^6$ , pressure increases in the turbulent flow near the front area of the second segment. This effect increases with increasing the distance between the bodies. The distributions of pressure and skin-friction coefficients, and heat flux along the surface of the second segment are shown in Figs. 10, 11, and 12 correspondingly. The extreme values of these parameters occur on the front surface of the segment. The pressure coefficient and heat flux in this area are larger than their values on the surface of the first segment by a factor of eight. The Reynolds number influences significantly the aerodynamic characteristics (skin-friction and heat flux). The geometrical factor (a distance between the bodies) influences pressure distribution in the front area of the second segment.

The flow behind the bodies remains turbulent at  $Re_{ar} \geq 10^6$  (see Fig. 13). The pressure distribution pattern in this case is different from the pattern of the laminar flow at  $Re_{ar} = 10^5$ . The increasing of the distance between the bodies results in increasing pressure in the rear local area behind the second segment. The area width can be estimated as  $2D$ .

### Summary

The hypersonic turbulent flow parameters near a two-segment projectile have been evaluated using an effective numerical algorithm. The turbulence significantly influences the distributions of the pressure, skin friction and heat flux along the projectile surfaces as well as the flow parameters in the wakes behind the segments. At  $Re_{ar} \geq 10^6$ , it has been found that the flow zone between the segments has become a fully recirculating subsonic flow. This effect is responsible for significant change of skin-friction and heat-flux characteristics along the second-segment surface.

### References

<sup>1</sup>Reinecke, W. G., and Legner, H. H., "A Review of Hypervelocity Projectile Aerophysics," *AIAA Paper*, No. 95-1853, June 1995.

<sup>2</sup>Cayzac, R., Tasset, B., Carette, E., Champigny, P., and

Bernhardt, J. M., "Aerothermodynamics of Hypersonic Projectiles," *AIAA Paper*, No. 95-1854, June 1995.

<sup>3</sup>Seiler, S., Legner, H. H., Miller, M. G., and Reinecke, W., "Impact of EM Effects on Hypervelocity Projectile Flight," *AIAA Paper*, No. 95-1852, June 1995.

<sup>4</sup>Orphal, D. L., and Franzen, R. R., "Penetration Mechanics and Performance of Segmented Rods Against Metal Targets," *International Journal of Impact Engineering*, Vol. 10, 1990, pp. 427-438.

<sup>5</sup>Yegorov, I. V., Yegorova, M. V., Ivanov, D. V., and Riabov, V. V., "Numerical Study of Hypersonic Viscous Flow About Plates Located Behind a Cylinder," *AIAA Paper*, No. 97-2573, June 1997.

<sup>6</sup>Yegorov, I. V., Yegorova, M. V., and Riabov, V. V., "Analysis of Hypersonic Viscous Flow About Bluff Cylinders Placed One After Another," *AIAA Paper*, No. 98-0171, January 1998.

<sup>7</sup>Yegorov, I. V., Ivanov, D. V., and Obabko, A., "Newton Technique in Numerical Simulation of Turbulent Flows," 1997.

<sup>8</sup>Bashkin, V. A., Egorov, I. V., and Egorova, M. V., "Supersonic Viscous Perfect Gas Flow Past a Circular Cylinder," *Fluid Dynamics*, No. 6, Nov.-Dec. 1993, pp. 833-838.

<sup>9</sup>Yegorov, I., and Zaitsev, O., "Development of Efficient Algorithms for Computational Fluid Dynamic Problems," *Proceedings of the Fifth International Symposium on Computational Fluid Dynamics*, Japan, Sendai, 1993, Vol. III, pp. 393-400.

<sup>10</sup>Coakley, T. J., and Huang, P. G., "Turbulence Modeling for High Speed Flows," *AIAA Paper*, No. 92-0436, January 1992.

<sup>11</sup>Ivanov, D. V., Obabko, A. V., and Yegorov, I. V., "Simulation of Separated Flows on the Base of Differential Turbulence Model," *AIAA Paper*, No. 97-1861, July 1997.

<sup>12</sup>Godunov, S. K., "Finite Difference Method for Numerical Computation of Discontinuous Solutions of the Equations of Fluid Dynamics," *Matematicheskii Sbornik*, Vol. 47, No. 3, 1959, pp. 271-306 (in Russian).

<sup>13</sup>Roe, P. L., "Approximate Riemann Solvers, Parameter Vectors, and Difference Scheme," *Journal of Computational Physics*, Vol. 43, 1981, pp. 357-372.

<sup>14</sup>Kolgan, V. P., "Application of the Principle of Minimum Value of Derivatives to the Construction of Finite-Difference Schemes for Calculating Discontinuous Solutions of Gas Dynamics," *Uchenye Zapiski TsAGI*, Vol. 3, No. 6, 1972, pp. 68-77 (in Russian).

<sup>15</sup>Yegorov, I. V., and Ivanov, D. V., "Application of the Complete Implicit Monotonized Finite-Differential Schemes in Modeling Internal Plane Flows," *Journal of*

*Computational Mathematics and Mathematical Physics*, Vol. 36, No. 12, 1996, pp. 91-107.

<sup>16</sup>Davis, R. T., "Numerical Methods for Coordinate Generation Based on Schwarz-Christoffel Transformations," AIAA Paper, No. 79-1463, June 1979.

<sup>17</sup>Bashkin, V. A., Yegorov, I. V., and Ivanov, D. V., "Application of Newton's Method to Calculation of Supersonic Internal Separation Flows," *Journal of Applied Mechanics and Technical Physics*, Vol.38, No.1, 1997, pp. 30-42.

<sup>18</sup>Karimov, T. Kh., "Some Iteration Methods for Solving Nonlinear Equations in the Hilbert's Space," *Doklady Akademii Nauk SSSR*, Vol. 269, No. 5, 1983, pp. 1038-1042 (in Russian).

<sup>19</sup>Lipton, R. J., Rose, D. J., and Tarjan, R. E., "Generalized Nested Dissection," *SIAM Journal of Numerical Analysis*, Vol. 16, No. 2, 1979, pp. 346-358.

<sup>20</sup>Egorov, I. V., and Zaitsev, O. L., "On an Approach to the Numerical Solution of the Two-Dimensional Navier-Stokes Equations by the Shock Capturing Method," *Journal of Computational Mathematics and Mathematical Physics*, Vol. 31, No. 2, 1991, pp. 286-299.

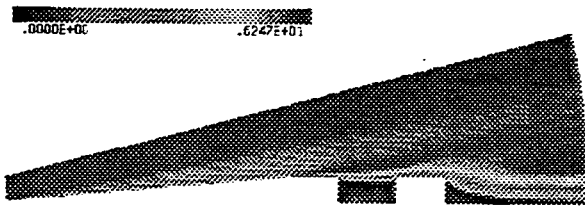


**Fig. 1** Mach number contours near a two-segment projectile at  $Re_r = 10^6$ ,  $M_\infty = 6$ .

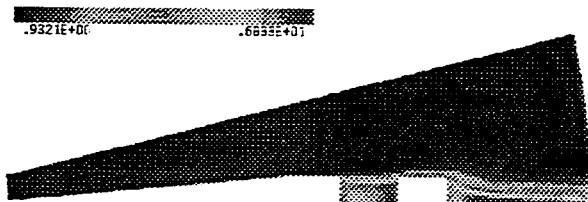


**Fig. 2** Temperature contours near a two-segment projectile at  $Re_r = 10^6$ ,  $M_\infty = 6$ .

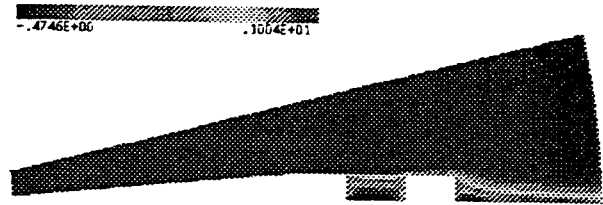


**Fig. 3** Velocity ( $u$ ) contours near a two-segment projectile at  $Re_r = 10^6$ ,  $M_\infty = 6$ .

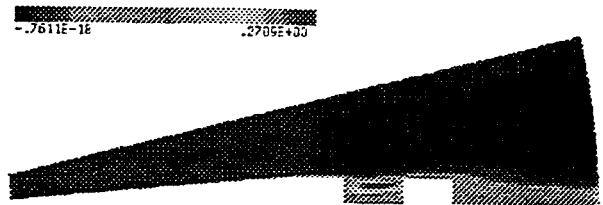


**Fig. 4** Turbulence  $g$ -parameter contours near a two-segment projectile at  $Re_r = 10^6$ ,  $M_\infty = 6$ .

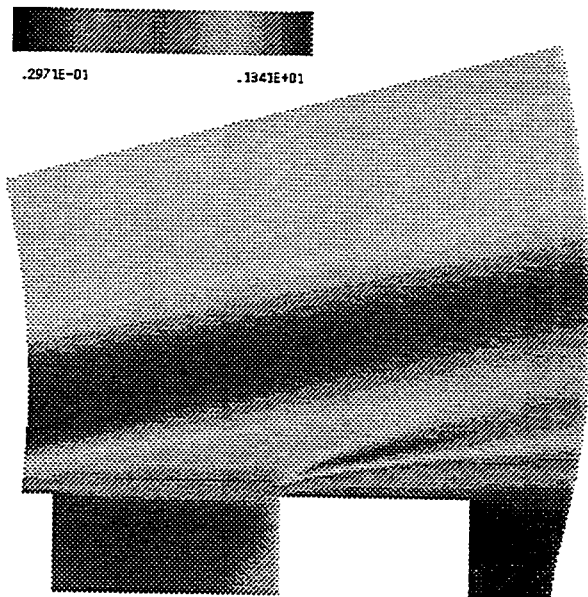


**Fig. 5** Density contours near a two-segment projectile at  $Re_r = 10^6$ ,  $M_\infty = 6$ .

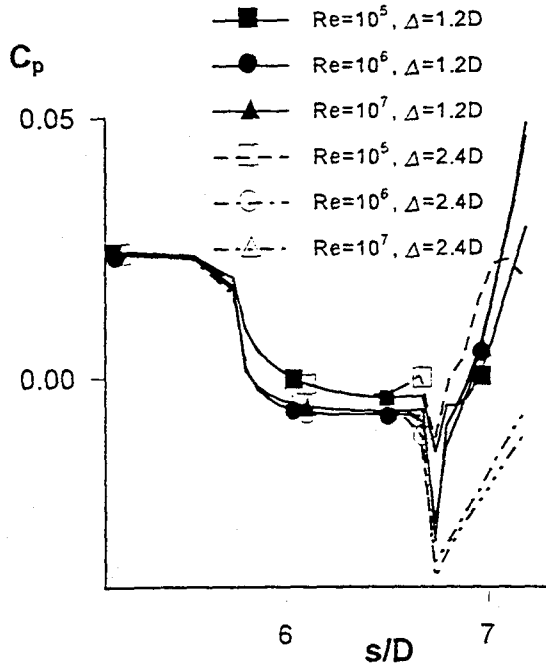


Fig. 6 Pressure coefficient ( $C_p$ ) distribution along the surface of the first segment.

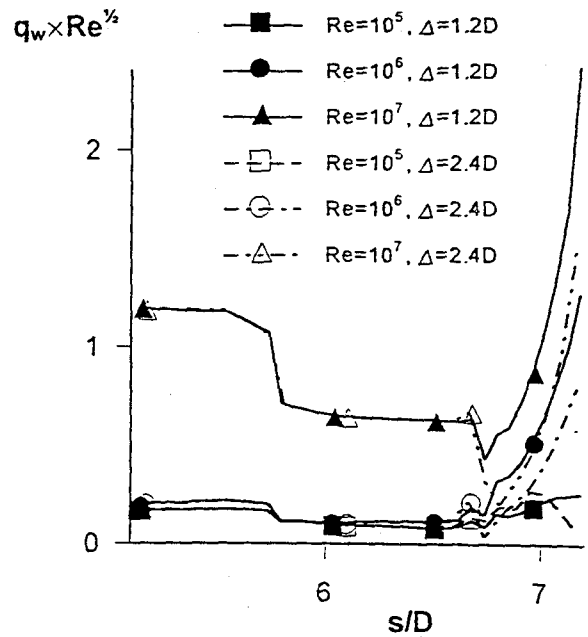


Fig. 8 Heat flux ( $q_w$ ) distribution along the surface of the first segment.

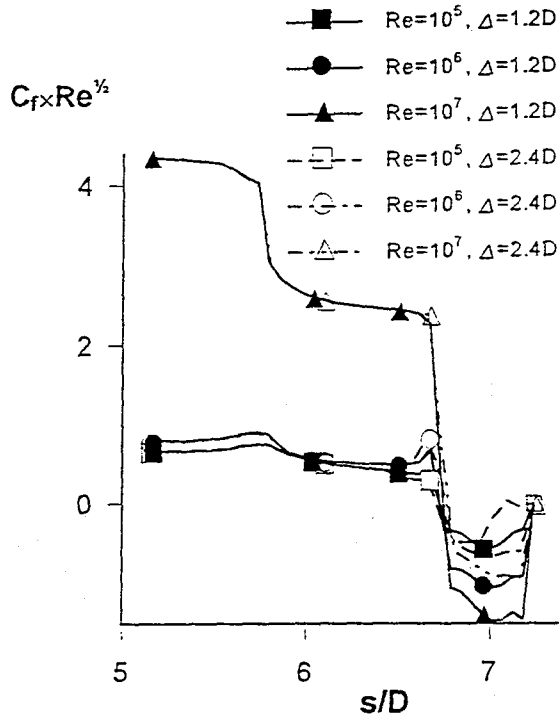


Fig. 7 Skin-friction coefficient ( $C_f$ ) distribution along the surface of the first segment.

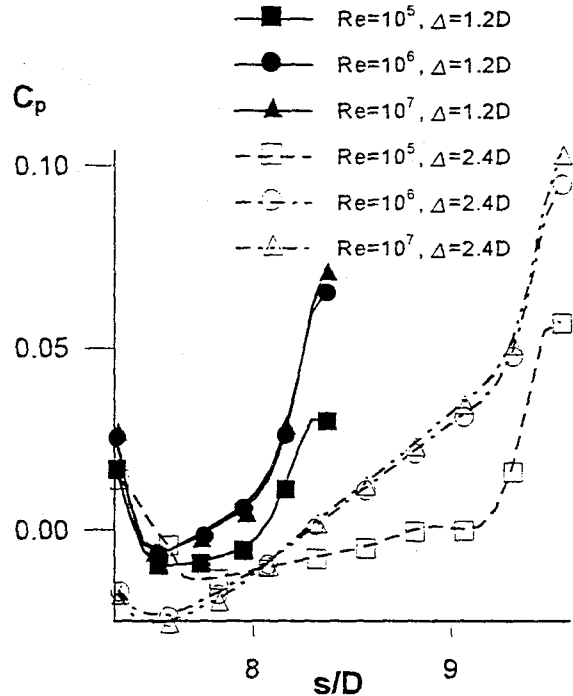


Fig. 9 Pressure coefficient ( $C_p$ ) distribution between the segments of the projectile.

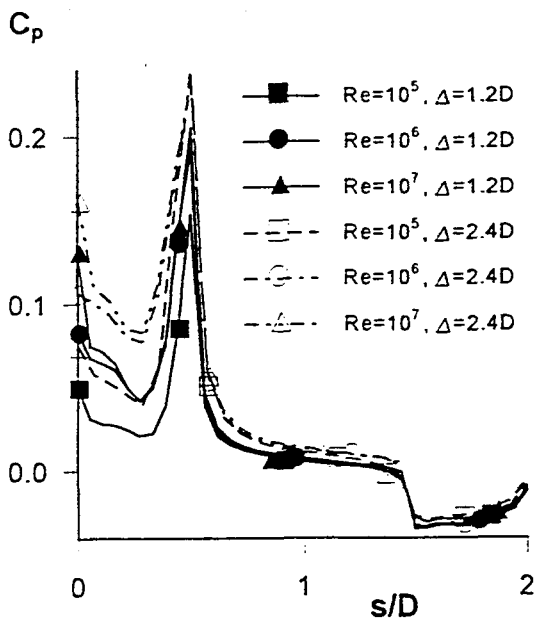


Fig. 10 Pressure coefficient ( $C_p$ ) distribution along the surface of the second segment.

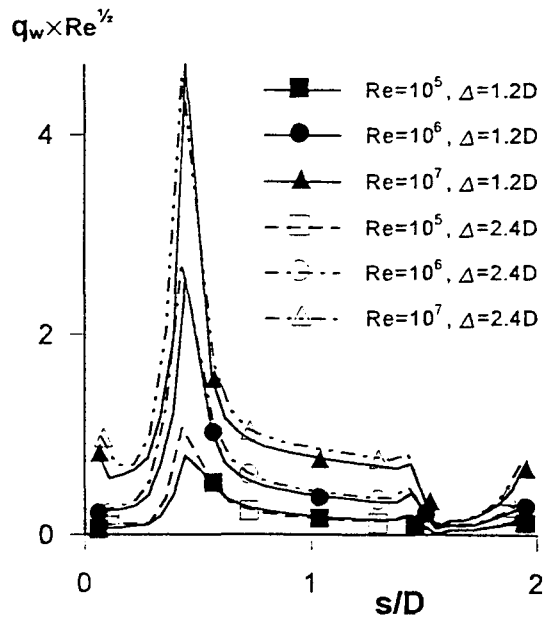


Fig. 12 Heat flux ( $q_w$ ) distribution along the surface of the second segment.

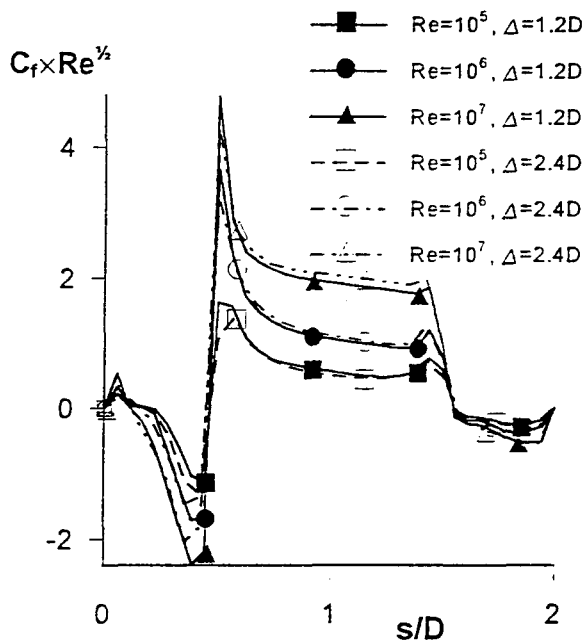


Fig. 11 Skin-friction coefficient ( $C_f$ ) distribution along the surface of the second segment.

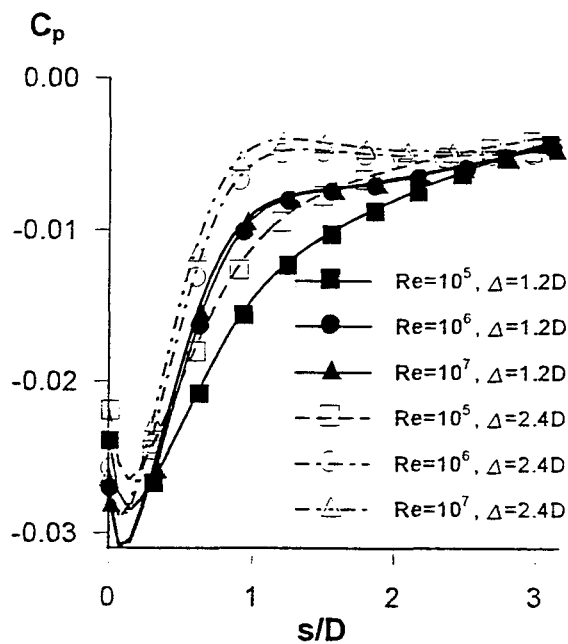


Fig. 14 Pressure coefficient ( $C_p$ ) distribution in the wake behind second segment.